Eurographics Symposium on Rendering (2025)
B. Wang and A. Wilkie (Editors)

Sharpening Your Density Fields: Spiking Neuron Aided Fast Geometry Learning

1. Supplemantary Materials

1.1. More Visual Results

Figures (1 3 4 5) show all visual comparisons between Nerfacto [TWN*23] and our method on the Blender dataset [MST*20]. Figures (6 7 8) present the results of Nerfacto and our approach on the DTU dataset [JDV*14]. The comprehensive visual comparisons show that our method achieves more accurate geometries compared to the Nerfacto baseline.

1.2. Reconstruction Results on Transparent Objects

To further exploit the practicality of our method, we implement our method based on Instant-NGP [MESK22] and conduct an experiment on 2 scenes of the transparent DexNeRF [IAKG20] datasets, shown in Fig. 2

1.3. Additional Ablation Study

As stated in the paper, the first term in Eq. 1 introduces ambiguity in the extracted geometry and incurs additional computational overhead. To further demonstrate our statement, we have conducted an additional ablation study on four scenes. The results in Tab. 1 indicate that dropping this term leads to a more accurate reconstruction of the geometry.

$$\frac{\partial \sigma_s}{\partial \sigma} = r * \max(0, \frac{k - |\sigma - \vartheta_{\text{th}}|}{k^2}) * \sigma + \Theta(\sigma - \vartheta_{\text{th}}), \qquad (1)$$

Table 1: *Ablation study on dropping the first term in Eq. 1.*

Scene	Scan40	Scan65	Scan106	Hotdog
w/o drop	0.87	0.99	0.98	1.12
w/ drop	0.81	0.91	0.74	0.69

1.4. Comparisons with Gaussian Splatting-based methods

Our approach focuses on NeRF-based geometry reconstruction. However, to further demonstrate the effectiveness, we also compare our proposed method with representative GS-based approaches, including 3DGS [KKLD23], SuGaR [GL24], G-Surfel [DXX*24], 2DGS [HYC*24], GOF [YSG24], and SpikingGS [ZLM*24], on both the Blender [MST*20] and the DTU [JDV*14] datasets. Experiments conducted on the Blender dataset in Tab. 2 demonstrate that our method outperforms all these GS-based methods, highlighting its effectiveness and superiority in geometry reconstruction. Comparative results on the DTU dataset, shown in Tab. 3, are suboptimal since the DTU dataset is captured from partial views, which results in the background being under-optimized in our method. Background modeling is beyond the scope of this work and is left for our future investigation.

Table 2: *Quantitative Comparisons on the Blender dataset [MST*20] with GS-based approaches. We measure the performance by Chamfer distance $\times 10^{-2}$. The **red** and **blue** numbers indicate the first and the second performer for each scene.*

Scene	Chair	Drums	Ficus	Hotdog	Lego	Mat.	Mic	Ship	Avg.
3DGS [KKLD23]	2.76	3.62	8.38	5.38	2.44	2.92	3.17	2.18	3.86
SuGaR [GL24]	0.67	1.08	0.57	1.42	0.73	0.95	0.87	1.19	0.94
G-Surfel [DXX*24]	0.75	**0.78**	**0.56**	1.77	0.93	1.08	0.99	2.35	1.15
2DGS [HYC*24]	**0.40**	1.83	0.66	1.41	0.87	0.93	1.13	**1.11**	1.04
GOF [YSG24]	1.23	1.33	0.59	1.18	**0.72**	**0.72**	0.70	1.35	0.98
SpikingGS [ZLM*24]	**0.45**	1.38	0.69	**1.13**	0.81	0.94	**0.61**	**0.96**	**0.87**
Ours	0.75	**0.63**	**0.43**	**0.69**	**0.64**	**0.41**	**0.40**	1.25	**0.65**

References

[DXX*24] DAI P., XU J., XIE W., LIU X., WANG H., XU W.: High-quality surface reconstruction using gaussian surfels. In *ACM SIGGRAPH 2024 Conference Papers* (2024), pp. 1–11. 1, 2

[GL24] GUÉDON A., LEPETIT V.: Sugar: Surface-aligned gaussian splatting for efficient 3d mesh reconstruction and high-quality mesh rendering. In *Proceedings of the IEEE/CVF Conference on Computer Vision and Pattern Recognition* (2024), pp. 5354–5363. 1, 2

[HYC*24] HUANG B., YU Z., CHEN A., GEIGER A., GAO S.: 2d gaussian splatting for geometrically accurate radiance fields. In *ACM SIGGRAPH 2024 conference papers* (2024), pp. 1–11. 1, 2

[IAKG20] ICHNOWSKI* J., AVIGAL* Y., KERR J., GOLDBERG K.: Dex-NeRF: Using a neural radiance field to grasp transparent objects. In *Conference on Robot Learning (CoRL)* (2020). 1, 2

[JDV*14] JENSEN R., DAHL A., VOGIATZIS G., TOLA E., AANÆS H.: Large scale multi-view stereopsis evaluation. In *Proceedings of the*

Table 3: *Quantitative Comparisons on the DTU dataset [JDV*14] with GS-based approaches. We measure the performance by Chamfer distance. The **red** and **blue** numbers indicate the first and the second performer for each scene.*

Scan	24	37	40	55	63	65	69	83	97	105	106	110	114	118	122	Avg.
3DGS [KKLD23]	2.14	1.53	2.08	1.68	3.49	2.21	1.43	2.07	2.22	1.75	1.79	2.55	1.53	1.52	1.50	1.96
SuGaR [GL24]	1.47	1.33	1.13	0.61	2.25	1.71	1.15	1.63	1.62	1.07	0.79	2.45	0.98	0.98	0.79	1.33
G-Surfel [DXX*24]	0.66	0.93	0.54	0.41	1.06	1.14	0.85	1.29	1.53	0.79	0.82	1.58	0.45	0.45	0.53	0.88
2DGS [HYC*24]	**0.48**	0.91	**0.39**	**0.39**	**1.01**	**0.83**	**0.81**	1.36	**1.27**	0.76	**0.70**	1.40	**0.40**	**0.40**	**0.52**	0.80
GOF [YSG24]	**0.52**	**0.91**	**0.40**	**0.37**	1.11	**0.88**	**0.72**	**1.18**	**1.26**	**0.75**	**0.72**	**0.88**	0.46	0.46	0.55	**0.76**
SpikingGS [ZLM*24]	0.63	**0.80**	0.50	0.46	1.04	1.01	0.87	**1.15**	1.32	**0.61**	0.73	**1.19**	**0.44**	**0.44**	**0.48**	**0.79**
Ours	0.94	1.25	0.81	0.48	**1.00**	0.90	1.14	1.21	1.70	1.17	0.73	1.33	1.14	0.85	0.53	0.94

Figure 1: *Reconstruction results on the Blender dataset [MST*20] (Chair, Drums).*

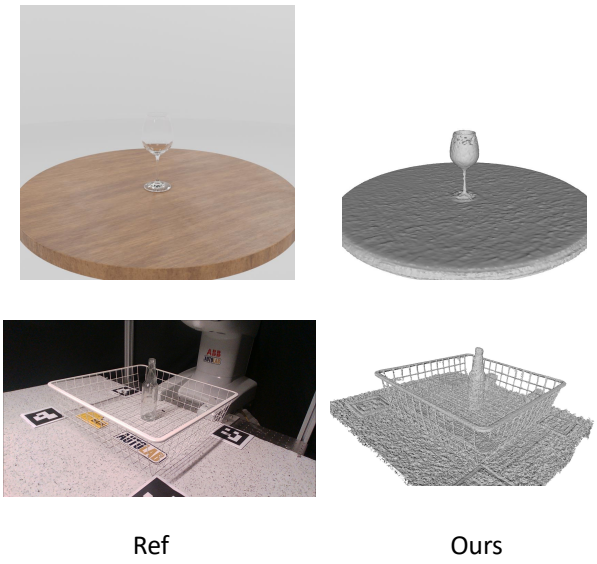

Figure 2: *Reconstruction results on the DexNeRF dataset [IAKG20]. The first row is a synthetic scene. The second row is a real-world case.*

IEEE Conference on Computer Vision and Pattern Recognition (2014), pp. 406–413. 1, 2, 5, 6, 7

[KKLD23] KERBL B., KOPANAS G., LEIMKÜHLER T., DRETTAKIS G.: 3d gaussian splatting for real-time radiance field rendering. *ACM Trans. Graph. 42*, 4 (2023), 139–1. 1, 2

[MESK22] MÜLLER T., EVANS A., SCHIED C., KELLER A.: Instant neural graphics primitives with a multiresolution hash encoding. *ACM Trans. Graph. 41*, 4 (July 2022), 102:1–102:15. URL: https://doi.org/10.1145/3528223.3530127, doi:10.1145/3528223.3530127. 1

[MST*20] MILDENHALL B., SRINIVASAN P. P., TANCIK M., BARRON J. T., RAMAMOORTHI R., NG R.: Nerf: Representing scenes as neural radiance fields for view synthesis. In *ECCV* (2020). 1, 2, 3, 4

[TWN*23] TANCIK M., WEBER E., NG E., LI R., YI B., WANG T., KRISTOFFERSEN A., AUSTIN J., SALAHI K., AHUJA A., ET AL.: Nerfstudio: A modular framework for neural radiance field development. In *ACM SIGGRAPH 2023 Conference Proceedings* (2023), pp. 1–12. 1

[YSG24] YU Z., SATTLER T., GEIGER A.: Gaussian opacity fields: Efficient adaptive surface reconstruction in unbounded scenes. *ACM Transactions on Graphics (TOG) 43*, 6 (2024), 1–13. 1, 2

[ZLM*24] ZHANG W., LI Z., MA D., TANG H., JIANG X., ZHENG Q., PAN G.: Spiking gs: Towards high-accuracy and low-cost surface re-

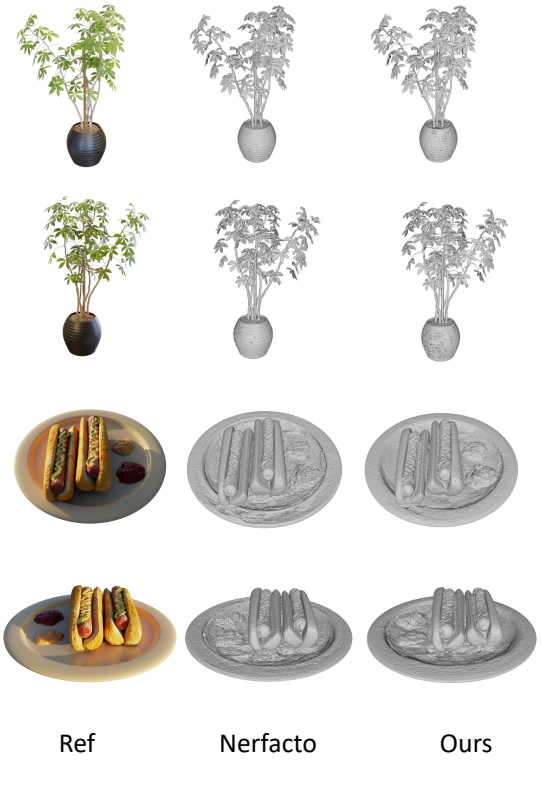

Figure 3: *Reconstruction results on the Blender dataset [MST* 20] (Ficus, Hotdog).*

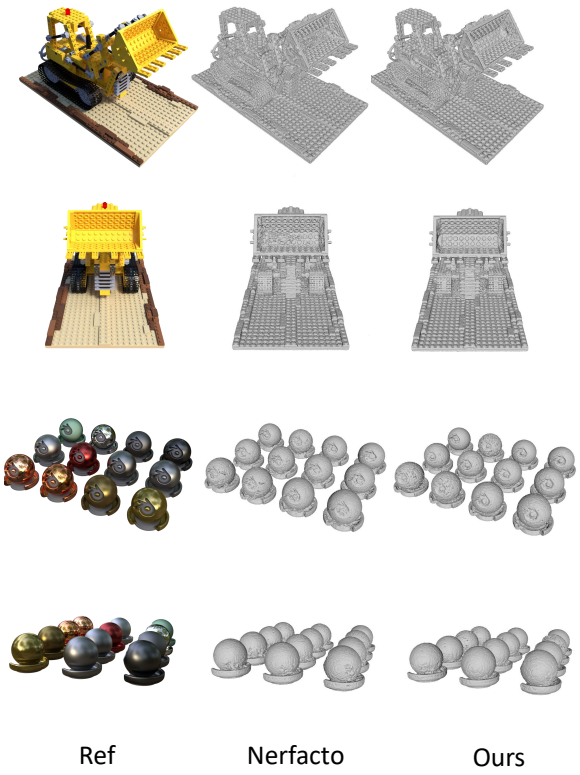

Figure 4: *Reconstruction results on the Blender dataset [MST* 20] (Lego, Materials).*

construction via spiking neuron-based gaussian splatting. *arXiv preprint arXiv:2410.07266* (2024). 1, 2

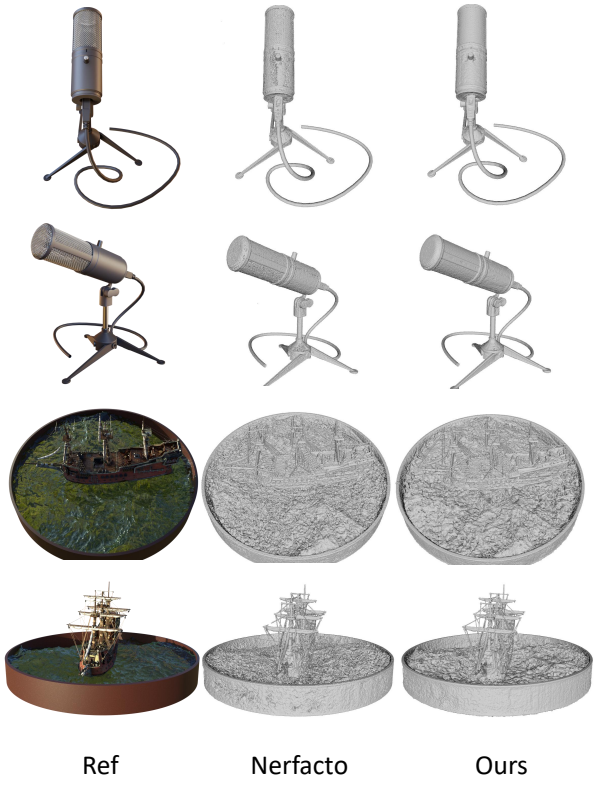

Figure 5: *Reconstruction results on the Blender dataset [MST* 20] (Mic, Ship).*

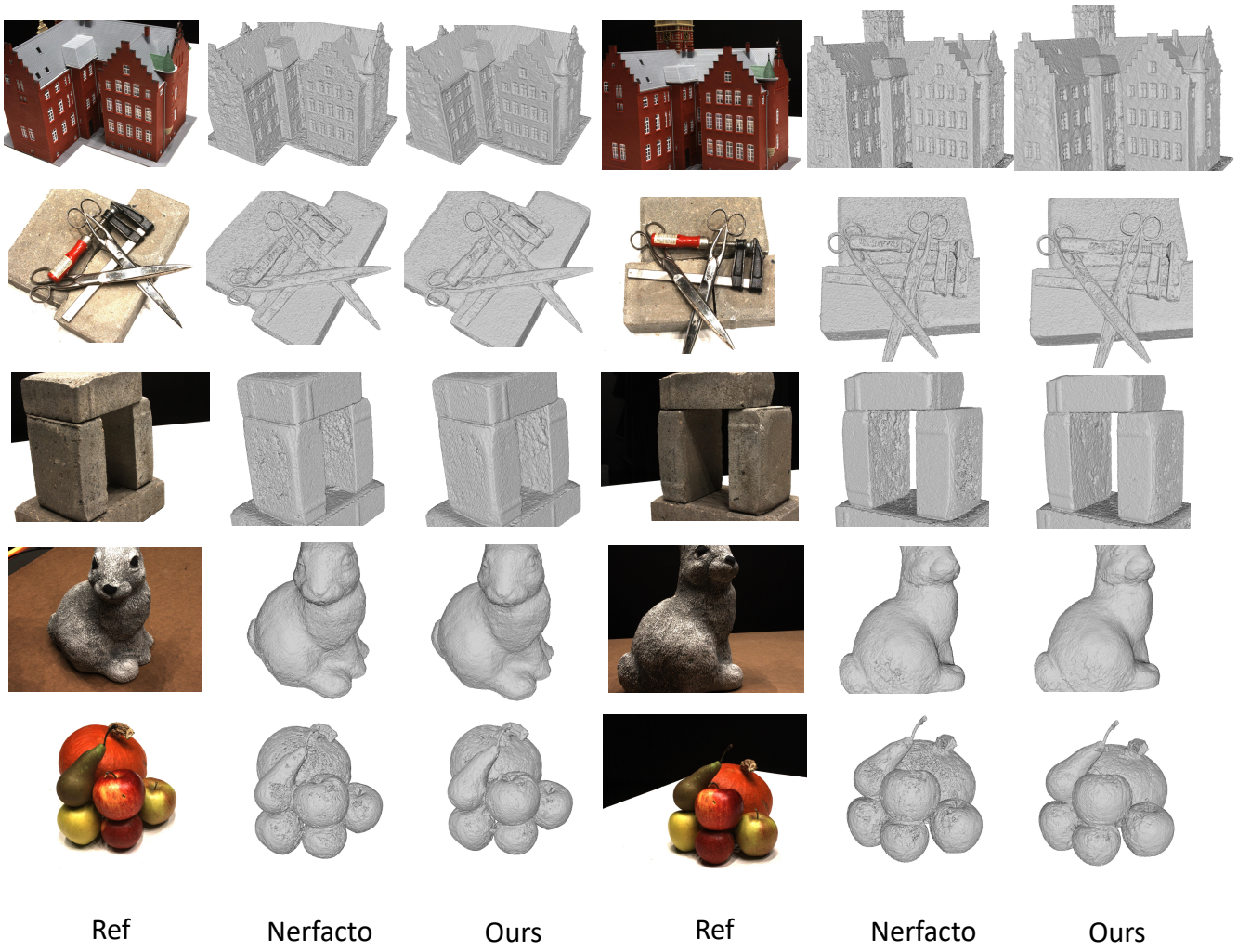

Figure 6: *Reconstruction results on the DTU dataset [JDV*14]. From top to bottom: Scan 24; Scan 37; Scan 40; Scan 55; Scan 63.*

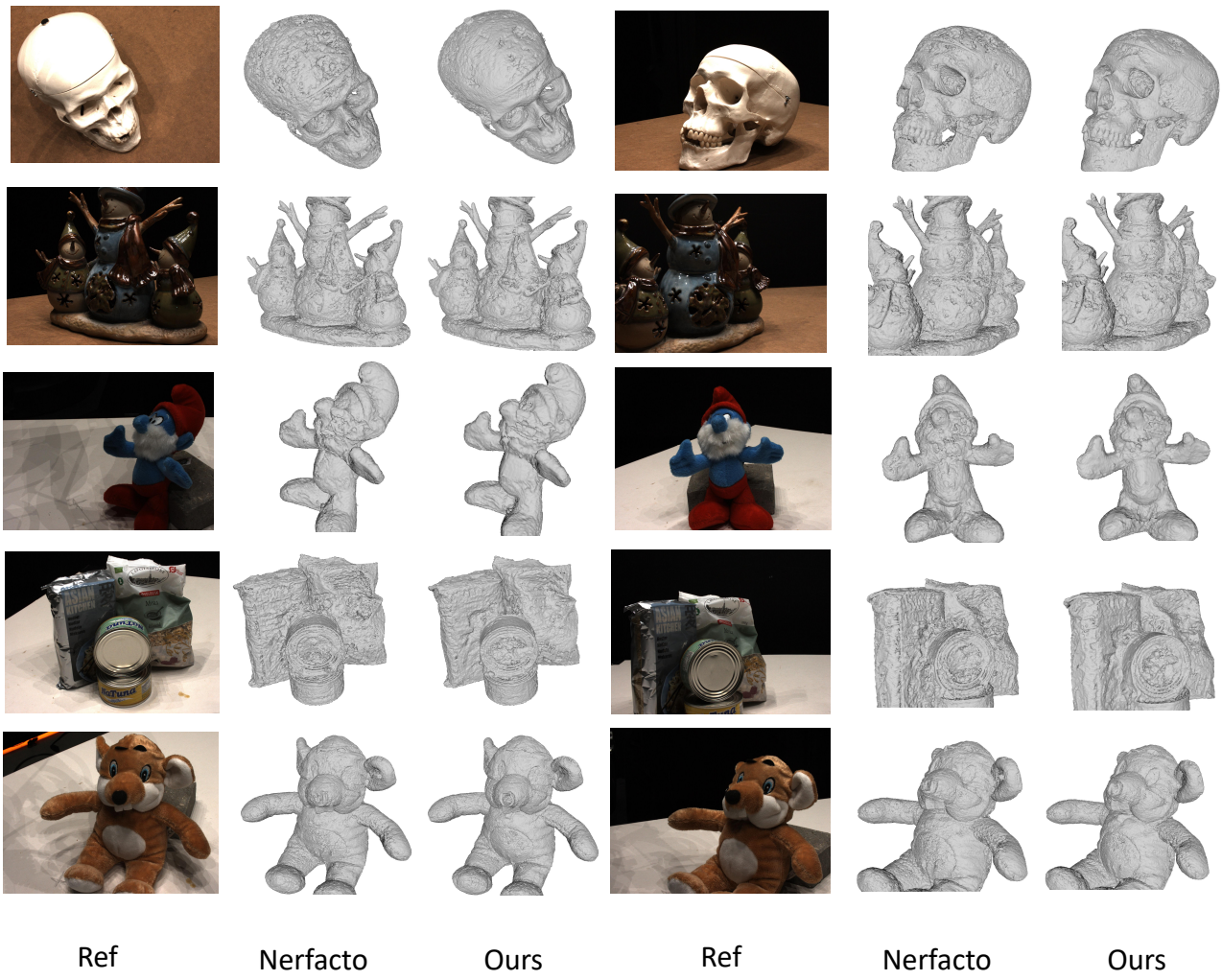

Figure 7: *Reconstruction results on the DTU dataset [JDV*14]. From top to bottom: Scan 65; Scan 69; Scan 83; Scan 97; Scan 105.*

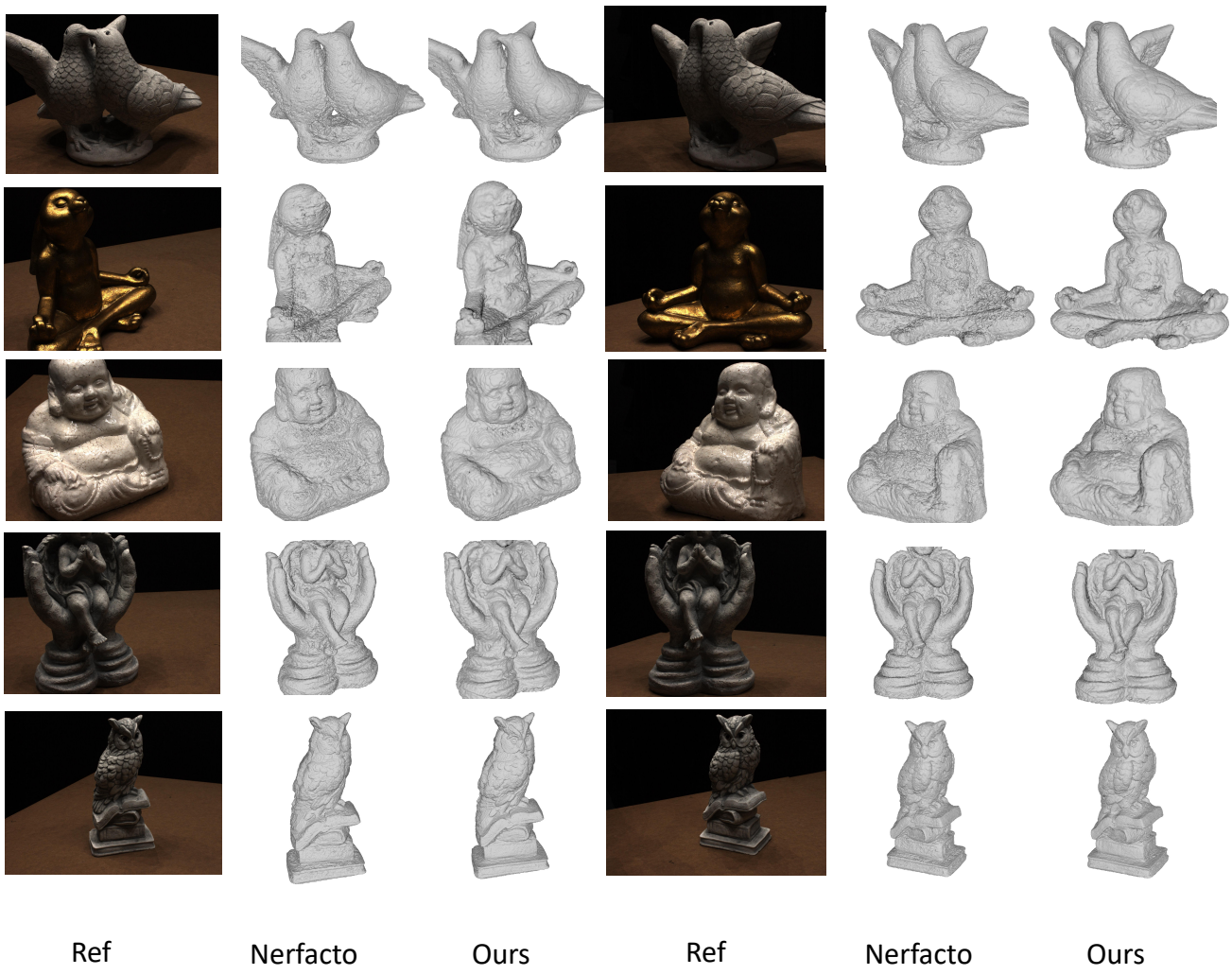

Figure 8: *Reconstruction results on the DTU dataset [JDV*14]. From top to bottom: Scan 106; Scan 110; Scan 114; Scan 118; Scan 122.*